

# Processive Catalytic Polymerization via Molecularly Confined Catalyst

## Authors:

Zefeng Zhou<sup>1</sup>, Wei-Shang Lo<sup>1</sup>, Gavin J. Giardino<sup>1</sup>, Kanika Lalit<sup>2</sup>, Wenqi Wang<sup>1</sup>, Chloe Fields<sup>1</sup>,  
Alfred Barney<sup>1</sup>, Chia-Kuang Tsung<sup>1</sup>, Wenyu Huang<sup>2,3\*</sup>, and Jia Niu<sup>1\*</sup>

## 5 Affiliations:

<sup>1</sup>Department of Chemistry, Boston College; Chestnut Hill, MA 02467, USA.

<sup>2</sup>Department of Chemistry, Iowa State University; Ames, IA 50011, USA.

<sup>3</sup>US Department of Energy, Ames National Laboratory; Ames, IA 50011, USA

\*Corresponding author. Email: [whuang@iastate.edu](mailto:whuang@iastate.edu); [jia.niu@bc.edu](mailto:jia.niu@bc.edu)

10

**Controlling the reactivity of the propagating chain end in polymerization reactions is crucial for achieving well-defined polymers in both synthetic polymer chemistry<sup>1,2</sup> and biology<sup>3</sup>. Processive enzymes in nature have evolved substrate-enclosing structures to protect the catalytic center from reaccess by the nascent polymer<sup>4</sup>. However, substrate enclosure has not**

15 **been adopted in polymer chemistry for improving catalytic processivity. Here, we present a strategy for processive catalytic polymerization by encapsulating catalysts for ring-opening metathesis polymerization (ROMP) into the sub-surface cages of a metal-organic framework. The sub-surface encapsulation of the catalysts within the framework protects**

the propagating polymer chain end from the secondary metathesis reaction with the alkenes in the backbone of the nascent polymer, while allowing the nascent polymer to grow out of the framework with little impedance and achieve continuous chain growth. As a result, ultra-high-molecular-weight polymers with low dispersity were generated from the ROMP of low-strain cyclic olefins such as *cis*-cyclooctene and cyclopentene. We demonstrate that ultra-high-molecular-weight polymers with degradable backbones and enhanced mechanical and adhesive properties could be readily generated from this approach.

Achieving precise control over molecular weight, dispersity, and polymer microstructures is a central goal in synthetic polymer chemistry<sup>5</sup>. Leveraging highly efficient metathesis catalysts, ring-opening metathesis polymerization (ROMP) of cyclic olefins has produced a plethora of functional polymers spanning synthetic elastomers and biomimetic polymers. In particular, high molecular weight polymers produced by ROMP have shown great promise in advanced applications such as the biomedical implants<sup>6</sup> and tribotechnical materials<sup>7</sup>. However, to date, only high-strain cyclic olefins (*e.g.*, norbornene, cyclobutene, etc.) can be polymerized by ROMP into polymers of high molecular weight and with living characteristics<sup>8-10</sup>. ROMP of cyclic olefins with low or moderate ring strain remains prone to secondary metathesis such as intramolecular backbiting and intermolecular chain transfer, leading to polymers with low molecular weight and broad dispersity that hindered their applications<sup>11,12</sup> (**Fig. 1a**). Due to the strong motivation to develop sustainable polymers, there is an urgent need for new ROMP techniques that can efficiently synthesize high molecular weight polymers from low-strain monomers that are either

derived from biobased feedstock, or consist of degradable moieties, or enable a circular polymerization-depolymerization life cycle<sup>13-15</sup>.

Enzymes with high catalytic processivity have evolved in nature to synthesize, degrade, and modify biopolymers. Processive enzymes remain bound to their polymeric substrates while performing multiple turnovers at high rates<sup>4</sup>. A widely conserved structural feature of processive enzymes is substrate enclosure, *i.e.*, polymer substrates/products are threaded through an enclosing motif such that they are restricted from reaccessing the catalytic center (**Fig. 1b**). Inspired by the substrate enclosure structures of processive enzymes, we envision that polymerization catalysts for ROMP (*e.g.*, Ru-based Grubbs catalysts) can be encapsulated into molecularly defined cages, where monomer molecules will be allowed to access the propagating chain end of the polymer that is associated with the catalysts, while the nascent polymer chains outside of the cages are prevented from reaccessing the catalyst (**Fig. 1c**). During polymerization, the cages serve as selective physical barriers that inhibit intramolecular backbiting and intermolecular chain transfer, resulting in high processivity and the production of polymers of high molecular weights. It is noteworthy that this molecularly confined catalyst system stands in stark contrast to the existing supported (such as polymer-supported and silica-supported) metathesis catalysts, which lack molecular confinement and do not reduce secondary metathesis<sup>16-20</sup>.

Metal-organic frameworks (MOFs), with their tunable cavity dimensions and chemical environment, are ideal candidates as molecularly defined cages for catalyst confinement<sup>21-22</sup>.

Importantly, multiple post-synthetic encapsulation methods have been developed to incorporate

complex molecules into MOFs<sup>23,24</sup>. Among these methods, the aperture-opening encapsulation approach developed by Tsung, Byers, and coworkers could achieve facile encapsulation of organometallic compounds while maintaining their structural integrity and reactivity<sup>25,26</sup>. In this approach, one linker of a MOF cage dissociates to “open” an aperture of a MOF cage in polar solvents, which allows a catalyst molecule to diffuse into the cage through the expanded aperture. After encapsulation of the guest molecule, the reassociation of the linker closes the expanded aperture, trapping the catalyst in the cage. When the solvent is switched to non-polar solvents (*e.g.*, dichloromethane), the ligand dissociation is inhibited, and the catalyst is stably encapsulated within the cage. Compared to other catalyst encapsulation strategies such as *de novo* synthesis<sup>27</sup> and passive diffusion<sup>28</sup>, the aperture-opening encapsulation approach achieves stable confinement of the guest molecule into the sub-surface layer of MOF with minimal leaching, while being broadly compatible with a variety of guest molecules. Critically, compared to bulk encapsulation, the sub-surface encapsulation allowed the nascent polymer to grow out of the framework with little impedance shortly after initiation, thus ensuring the continuous chain growth and high processivity.

**Catalyst encapsulation and validation.** UiO-type MOFs were chosen as the host because of their superior thermal, chemical, and mechanical stabilities, and their versatility for post-synthetic encapsulation of guest molecules<sup>29</sup>. The encapsulation of Hoveyda-Grubbs second-generation catalyst (HG2) and the third-generation Grubbs catalyst (G3) into the cages in UiO-66 and UiO-67 using the aperture-opening encapsulation approach was investigated. The sizes of octahedral cages in UiO-66 (~10.7 Å) and UiO-67 (~15.6 Å)<sup>30</sup> are estimated to be slightly larger than the

size of HG2 (14.3 Å × 10.7 Å × 6.5 Å) and G3 (14.3 Å × 9.4 Å × 6.5 Å). Meanwhile, the sizes of triangular windows of the octahedral cages in UiO-66 (~8.3 Å) and UiO-67 (~11.1 Å) are smaller than the size of HG2 and G3, such that leaching of the encapsulated catalysts is prevented after the aperture is closed (**Fig. 2a** and **fig. s1**). The aperture-opening encapsulation was performed by first incubating the catalysts and the MOFs in acetonitrile at room temperature for 72 hours for HG2 or 24 hours for G3, before the solvent was switched to dichloromethane to keep the apertures closed. Furthermore, alternating dichloromethane wash and short sonication cycles were repeated six times to remove physically adsorbed catalysts on the exterior of the MOFs. <sup>1</sup>H NMR spectroscopy confirmed that HG2 and G3 remained stable under the encapsulation and washing conditions (**fig. s2**). The crystallinity, morphology, size, and porosity of both UiO-66 and UiO-67 before and after the encapsulation procedure remain largely unchanged, evidenced by powder X-ray diffraction (PXRD), scanning electron microscopy (SEM), transmission electron microscopy (TEM), and Brunauer-Emmett-Teller (BET) surface area analysis (**figs. s3-s6**). The ruthenium loading after encapsulation for four different encapsulated catalysts, namely HG2@UiO-66, HG2@UiO-67, G3@UiO-66, and G3@UiO-67, was determined by ICP-OES to be 0.020~0.10 wt% (**Fig. 2b**). UiO-67 with larger cages were found to encapsulate ~40% more of both Ru-based catalysts than UiO-66. The catalytic activities of the encapsulated catalysts were evaluated using a ring-closing metathesis (RCM) reaction of diallyl ether (**1**) (**Fig. 2b** and **table s1**). Under the same catalyst loading, HG2@UiO-67 and G3@UiO-67 showed markedly higher turnover frequency (TOF) in the RCM reaction than HG2@UiO-66 and G3@UiO-66 suggesting the larger cage of UiO-67

enabled better mass transport and provided adequate space for the encapsulated catalyst to interact with the substrate.

To confirm that the catalyst has been encapsulated into the cage rather than physically adsorbed on the exterior of the MOF matrix, we constructed a control catalyst, HG2/UiO-67, by subjecting  
5 UiO-67 and HG2 in dichloromethane in which the aperture remains closed. Following the same washing process and loading measurement, the HG2/UiO-67 was found to exhibit 0.0031 wt % of Ru loading, which is two orders of magnitude lower than HG2@UiO-67. Furthermore, no RCM reactivity was observed for HG2/UiO-67 (**table s2**). These results suggest that the washing procedure can efficiently remove the physically adsorbed catalyst and that the aperture-opening  
10 encapsulation procedure could indeed encapsulate metathesis catalysts into the cage of UiO-type MOFs.

Size-selectivity is a hallmark of MOF-encapsulated catalysts<sup>31-33</sup>. When subjected to tertiary amine inhibitors of different sizes, HG2@UiO-67 and free HG2 demonstrated distinct properties. While trimethylamine could inhibit both HG2@UiO-67 and HG2 effectively, HG2@UiO-67 became  
15 significantly more resistant to tertiary amines with longer alkyl substitutions, exhibiting 2.9- to 7.8-folds higher activity in the model RCM reaction after being exposed to tertiary amines with ethyl substitutions or longer (**Fig. 2c** and **table s3**). It is noteworthy that, unlike HG2@UiO-67, HG2/UiO-67 did not exhibit significant resistance to tertiary amine inhibitors. Furthermore, two RCM substrates of different sizes, diallylmalonate (**2**) and dihexyl 4,4'-((allyl(4-  
20 (allyl(hydrosulfonyl)amino)but-2-yn-1-yl)amino)sulfonyl)dibenzoate (**3**), were subjected to either

HG2 or HG2@UiO-67 (**Fig. 2d**). The observed rate constant of **2** was 1.3-fold higher than that of **3** when the reactions were catalyzed by free HG2 (**Fig. 2e** and **table s4**). In contrast, this ratio increased to 13.3 when the reactions were catalyzed by HG2@UiO-67 (**Fig. 2f**). Taken together, these results can all be attributed to the impedance of the diffusion of large molecules by the MOF cage, thereby confirming that the catalyst has indeed been encapsulated within the MOF cage in HG2@UiO-67.

**ROMP of low-strain cyclic olefins by MOF-encapsulated catalysts.** We first examined the ROMP of *cis*-cyclooctene, a model cyclic olefin with low ring strain. It has been well-documented that the ROMP of *cis*-cyclooctene suffers excessive secondary metathesis because of its low ring strain<sup>34,35</sup>. To investigate if the catalyst processivity in the ROMP of *cis*-cyclooctene could be improved through MOF encapsulation of the catalyst, we performed this reaction using two MOF-encapsulated catalysts, HG2@UiO-67 and G3@UiO-67. While HG2@UiO-67 resulted in a two-fold improvement of molecular weight and a modest reduction in dispersity (**fig. s7** and **table s5**), it did not improve the control over the polymerization as the molecular weight remained constant regardless of the conversion. The lack of control could be attributed to the slow rate of initiation of HG2 in ROMP than the rate of propagation, leading to disparate lengths of polymer chains<sup>36,37</sup>. In contrast, the reaction mediated by fast-initiating G3@UiO-67 exhibited living characteristics including first-order kinetics to the monomer, linear growth of molecular weight of the resulting polyoctenamer versus the conversion, and low dispersity ( $D = 1.13$ ), in addition to producing ultra-high molecular weight polyoctenamers up to  $M_n = 1,219$  kg/mol (**Fig. 3a–c**). Meanwhile, free G3 under the same condition and at similar conversion produced a polyoctenamer with much lower

molecular weight ( $M_n = 81$  kg/mol) and higher dispersity ( $D = 1.91$ ) (**Fig. 3d**). It is noteworthy that the addition of an exogenous ligand 3-bromopyridine was necessary to suppress the fast dissociation of the pyridinyl ligand of G3 and maintain the structural integrity of the cage-encapsulated G3. We also confirmed that the ROMP reaction was mediated by the MOF-encapsulated catalysts, rather than active catalysts leaching into the solution from the MOF. When the G3@UiO-67 solid was separated from the ROMP reaction of *cis*-cyclooctene, monomer conversion in the supernatant completely halted, suggesting that no active catalyst was leached into the supernatant (**Fig. 3e**).

Next, we applied G3@UiO-67 to the copolymerization of *cis*-cyclooctene and *cis*-4,7-dihydro-1,3-dioxepin (DXP), a comonomer that incorporates degradable motifs in the polymer backbone. Consistent with the result from the homopolymerization, copolymers with ultra-high molecular weight and low dispersity ( $M_n = 757$  kg/mol,  $D = 1.19$ ) were generated, compared to the counterpart generated by free G3 at similar conversions ( $M_n = 58$  kg/mol,  $D = 1.57$ ) (**Fig. 3f, 3g** and **table s6**). Furthermore, the copolymer generated by G3@UiO-67 incorporated 3-fold more DXP (0.74% vs. 0.24%), improving the degradability of the copolymer (**Fig. 3h, s11** and **table s7**).

Due to the low ceiling temperature of cyclopentene, polypentenamer can readily undergo depolymerization to generate cyclopentene under ambient conditions in the presence of metathesis catalysts<sup>38</sup>. In addition, the low ring strain of cyclopentene and the high propensity for secondary metathesis further exacerbate the challenges for ROMP. We reasoned that the MOF cage would

serve as a physical barrier for the nascent polypentenamer to reaccess the catalyst and kinetically inhibit both the secondary metathesis and depolymerization during the ROMP of cyclopentene, allowing this reaction to become processive. Indeed, we found that the depolymerization of a purified polypentenamer ( $M_n = 355$  kg/mol,  $D = 1.91$ ) was inhibited when it was incubated with G3@UiO-67 in a dilute solution (0.1 M in THF) at 22 °C (**Fig. 4a** and **table s8**). In contrast, free G3 under the same condition led to fast depolymerization evidenced by  $^1\text{H}$  NMR (**Fig. 4b**) and SEC (**Fig. 4c**). Consistently, the ROMP of cyclopentene mediated by G3@UiO-67 yielded polypentenamer with ultra-high molecular weight and low dispersity ( $M_n = 532$  kg/mol,  $D = 1.40$ ) compared to the reaction mediated by free catalyst under the same condition ( $M_n = 67$  kg/mol,  $D = 3.60$ ) (**Fig. 4d** and **table s9**).

Taken together, the stark contrast between the reactions mediated by the MOF-encapsulated catalysts and those that are mediated by the free catalysts confirmed that the MOF cage could serve as an effective physical barrier to inhibit the secondary metathesis in ROMP and promote processive polymerization in the ROMP of low-strain cyclic olefins.

**Mechanical and adhesive properties of the polymer generated by MOF-encapsulated catalysts.** Molecular weight profoundly impacts the mechanical and adhesive properties of polymers. High molecular weight polymers typically demonstrate higher toughness and stronger adhesion than their low molecular weight counterparts because of increased chain entanglements<sup>39,40</sup>. We envisioned that the processive ROMP mediated by MOF-encapsulated catalysts could be readily applied to producing ultra-high molecular weight polymers with

improved mechanical and adhesive performance. To this end, we investigated the synthesis of ultra-high molecular weight poly(vinyl acetate-co-ethylene), p(VAE) via ROMP of 3-acetoxy *cis*-cyclooctene (3AcCOE), followed by hydrogenation to saturate the internal alkenes (**Fig. 5a**). Zhang *et al.*<sup>41</sup> demonstrated that ROMP of 3AcCOE could produce a regio-regular p(VAE) with an acetoxy group on every 8<sup>th</sup> carbon on the backbone that is mechanically superior to the polymer produced through the free radical polymerization of ethylene and vinyl acetate<sup>42</sup> or the coordination-insertion polymerization of these vinyl monomers<sup>43-45</sup>. Using G3@UiO-67, we synthesized an ultra-high molecular weight regio-regular p(VAE) ( $M_n = 907$  kg/mol,  $D = 1.33$ ) via ROMP of 3AcCOE and hydrogenation, which is, to our best knowledge, the highest molecular weight of p(VAE) recorded to date. After hydrogenation, this ultra-high molecular weight p(VAE) demonstrated typical thermoelastic behaviors with a strong strain hardening effect, achieving high ultimate stress ( $52 \pm 4$  MPa), high strain ( $750 \pm 44\%$ ), and an overall toughness ( $181 \pm 24$  MJ/m<sup>3</sup>) comparable to high-density polyethylene (HDPE) and isotactic polypropylene (*i*PP) (**Fig. 5b, 5c**). Notably, these mechanical properties are markedly higher than those ( $33 \pm 2$  MPa ultimate stress and  $152 \pm 10$  MJ/m<sup>3</sup> toughness) of a lower molecular weight regio-regular p(VAE) synthesized by the free catalyst ( $M_n = 37$  kg/mol,  $D = 2.10$ ). It is noteworthy that the commercial random copolymer of vinyl acetate and ethylene with 50 wt% VAc incorporation, p(VAE50), demonstrated completely different mechanical properties as a ductile elastomer ( $9 \pm 0.3$  MPa ultimate stress and  $63 \pm 3$  MJ/m<sup>3</sup> toughness).

Finally, the adhesive property of poly(vinyl acetate-*co*-vinyl alcohol-*co*-ethylene) (p(VAVAE)), generated by the partial deprotection of the regio-regular p(VAE), was measured by the lap shear test of a single-lap joint of polymer adhesive between two stainless steel slides. The ultra-high molecular weight p(VAVAE) ( $M_n = 990$  kg/mol, OH content: 18%) demonstrated 6.5-fold higher lap shear strength than the low molecular weight p(VAVAE) ( $M_n = 30$  kg/mol, OH content: 22%), with apparent lap shear strengths of  $1.12 \pm 0.23$  MPa and  $0.17 \pm 0.08$  MPa, respectively (Fig. 5d and table s15). This result further supports the strong chain entanglement of the ultra-high molecular polymer generated by the MOF-encapsulated catalyst than cannot be achieved by the low molecular weight counterpart produced by the free catalyst. Additionally, p(VAVAE)-990kg/mol also exhibited significantly enhanced adhesion to stainless steel compared to either HDPE ( $0.057 \pm 0.028$  MPa) or iPP ( $0.042 \pm 0.026$  MPa), surpassing their adhesion strength by more than an order of magnitude (Fig. 5d).

In summary, we developed a novel strategy for processive ROMP using MOF-encapsulated catalysts. Ru-based olefin metathesis catalysts were efficiently encapsulated into MOF cages via the aperture-opening encapsulation method. The catalysts demonstrated excellent activities and size selectivity in a model RCM reaction, suggesting successful encapsulation into MOFs. ROMP of *cis*-cyclooctene and DXP exhibited high processivity and living characteristics when the MOF-encapsulated catalyst G3@UiO-67 was employed, leading to polymers with ultra-high molecular weight and low dispersity. ROMP of cyclopentene mediated by G3@UiO-67 achieved significantly higher molecular weight and lower dispersity than the counterpart mediated by the free catalyst. The ultra-high molecular weight polymers generated by the encapsulated catalysts

demonstrated significantly improved mechanical and adhesive properties compared to the low molecular weight counterparts and commercial polymers. The simplicity and generality make this method readily applicable to the ROMP of a wide range of low-strain cyclic olefins. This work also revealed that molecular confinement is a promising strategy to reduce undesired chain transfer events in the polymerization mediated by other metalloorganic initiators.

## References:

1. Bielawski, C. W. & Grubbs, R. H. Living ring-opening metathesis polymerization, *Prog. Polym. Sci.* **32**, 1-29 (2007).
2. Wu, L. et al. Regulating cationic polymerization: From structural control to life cycle  
5 management. *Prog. Polym. Sci.* **145**, 101736 (2023).
3. Li, Y., Mitaxov, V. & Waksman, G. Structure-based design of *Taq* DNA polymerases with improved properties of dideoxynucleotide incorporation. *Proc. Natl. Acad. Sci.* **96**, 9491-9496, (1999).
4. Breyer, W. A. & Matthews, B. W. A Structural Basis for Processivity. *Protein Science* **10**,  
10 1699–1711 (2001).
5. Storey, R. F. Chapter 2: Fundamental Aspects of Living Polymerization, *Fundamentals of Controlled/Living Radical Polymerization* pp. 60–77, RSC Publishing, (2013).
6. Macuvele, D. L. P., et al. Advances in ultra-high molecular weight  
polyethylene/hydroxyapatite composites for biomedical applications: A brief review. *Mater. Sci. Eng. C* **76**, 1248-1262 (2017).  
15
7. Teplov, A. A., et al. Tribological, Physicomechanical, and Other Properties of Composites Based on Ultra-High Molecular-Weight Polyethylene, Polytetrafluoroethylene, and Ethylene–Tetrafluoroethylene Copolymer with Quasicrystalline Filler Al–Cu–Fe. *Crystallogr. Rep.* **66**, 883-896 (2021).

8. Slugovc, C. The Ring Opening Metathesis Polymerisation Toolbox. *Macromol. Rapid Commun.* **25**, 1283-1297 (2004).
9. Miyake, G. M., Weitekamp, R. A., Piunova, V. A. & Grubbs, R. H. Synthesis of Isocyanate-Based Brush Block Copolymers and Their Rapid Self-Assembly to Infrared-Reflecting Photonic Crystals. *J. Am. Chem. Soc.* **134**, 14249–14254 (2012).
10. Yang, J., et al. Bicyclohexene-peri-naphthalenes: Scalable Synthesis, Diverse Functionalization, Efficient Polymerization, and Facile Mechanoactivation of Their Polymers. *J. Am. Chem. Soc.* **142**, 14619–14626 (2020).
11. Steinbach, T., Alexandrino, E. M. & Wurm, F. R. Unsaturated poly(phosphoester)s via ring-opening metathesis polymerization. *Polym. Chem.* **4**, 3800-3806 (2013).
12. Debsharma, T., Behrendt, F. N., Laschewsky, A. & Schlaad, H. Ring-Opening Metathesis Polymerization of Biomass-Derived Levoglucosenol. *Angew. Chem. Int. Ed.* **58**, 6718-6721 (2019).
13. Miller, S. A. Sustainable Polymers: Opportunities for the Next Decade. *ACS Macro Lett.* **2**, 550–554 (2013).
14. Miller, S. A. Sustainable polymers: replacing polymers derived from fossil fuels. *Polym. Chem.* **5**, 3117-3118 (2014).
15. Sun, H., Liang, Y., Thomsson, M. P. & Gianneschi, N. C. Degradable polymers via olefin metathesis polymerization. *Progress in Polymer Science* **120**, 101427 (2021).

16. Nguyen, S. T. & Grubbs, R. H. The syntheses and activities of polystyrene-supported olefin metathesis catalysts based on  $\text{Cl}_2(\text{PR}_3)_2\text{Ru}=\text{CH}-\text{CH}=\text{CPh}_2$ . *J. Organomet. Chem.* **497**, 195-200 (1995).
17. Al-Hashimi, M., Tuba, R., Bazzi, H. S. & Grubbs, R. H. Synthesis of Polypentenamer and Poly(Vinyl Alcohol) with a Phase-Separable Polyisobutylene-Supported Second-Generation Hoveyda–Grubbs Catalyst. *ChemCatChem* **8**, 228–233 (2016).
18. Herrmann, W. A., et al. A Molecularly Defined, Grafted Olefin Metathesis Catalyst from Tris(neopentyl)-nitridomolybdenum(VI). *Angew. Chem. Int. Ed.* **35**, 2803-2805 (1996).
19. Yoon, K., et al. Scalable and continuous access to pure cyclic polymers enabled by ‘quarantined’ heterogeneous catalysts. *Nat. Chem.* **14**, 1242-1248 (2022).
20. Suriboot, J., Bazzi, H. S. & Bergbreiter, D. E. Supported Catalysts Useful in Ring-Closing Metathesis, Cross Metathesis, and Ring-Opening Metathesis Polymerization. *Polymer* **8**, 140 (2016).
21. Bavykina, A., Kolobov, N., Khan, S., Bau, J. A., Ramirez, A. & Gascon, J. Metal–Organic Frameworks in Heterogeneous Catalysis: Recent Progress, New Trends, and Future Perspectives. *Chem. Rev.* **120**, 8468–8535 (2020).
22. Liu, J., et al. MOF-enabled confinement and related effects for chemical catalyst presentation and utilization. *Chem. Soc. Rev.* **51**, 1045-1097 (2022).

23. Kumar, S., Mohan, B., Tao, Z., You, H. & Ren, P. Incorporation of homogeneous organometallic catalysts into metal–organic frameworks for advanced heterogenization: a review. *Catal. Sci. Technol.* **11**, 5734–5771 (2021).
24. Kalaj, M. & Cohen, S. M. Postsynthetic Modification: An Enabling Technology for the Advancement of Metal–Organic Frameworks. *ACS Cent. Sci.* **6**, 1046–1057 (2020).
25. Morabito, J. V., et al. Molecular Encapsulation beyond the Aperture Size Limit through Dissociative Linker Exchange in Metal–Organic Framework Crystals. *J. Am. Chem. Soc.* **136**, 12540–12543 (2014).
26. Li, Z., Rayder, T. M., Luo, L., Byers, J. A. & Tsung, C. Aperture-Opening Encapsulation of a Transition Metal Catalyst in a Metal–Organic Framework for CO<sub>2</sub> Hydrogenation. *J. Am. Chem. Soc.* **140**, 8082–8085 (2018).
27. Kaye, S. S. & Long, J. R. Matrix Isolation Chemistry in a Porous Metal–Organic Framework: Photochemical Substitutions of N<sub>2</sub> and H<sub>2</sub> in Zn<sub>4</sub>O[(η<sup>6</sup>-1,4-Benzenedicarboxylate)Cr(CO)<sub>3</sub>]<sub>3</sub>. *J. Am. Chem. Soc.* **130**, 806–807 (2008).
28. Chołuj, A., Zieliński, A., Grela, K. & Chmielewski, M. J. Metathesis@MOF: Simple and Robust Immobilization of Olefin Metathesis Catalysts inside (Al)MIL-101-NH<sub>2</sub>. *ACS Catal.* **6**, 6343–6349 (2016).
29. Cavka, J. H., et al. A New Zirconium Inorganic Building Brick Forming Metal Organic Frameworks with Exceptional Stability. *J. Am. Chem. Soc.* **130**, 1385013851 (2008).

30. Chavan, S., et al. H<sub>2</sub> Storage in Isostructural UiO-67 and UiO-66 MOFs. *Phys. Chem. Chem. Phys.* **14**, 1614-1626 (2012).
31. Zhang, W., et al. A Family of Metal-Organic Frameworks Exhibiting Size-Selective Catalysis with Encapsulated Noble-Metal Nanoparticles. *Adv. Mater.* **26**, 4056–4060 (2014).
- 5 32. Lee, J., et al. Metal–Organic Framework Materials as Catalysts. *Chem. Soc. Rev.* **38**, 1450-1459 (2009).
33. Lo, W., et al. Probing the Interface between Encapsulated Nanoparticles and Metal–Organic Frameworks for Catalytic Selectivity Control. *Chem. Mater.* **33**, 1946–1953 (2021).
34. Martinez, H., Ren, N., Matta, M. E. & Hillmyer, M. A. Ring-Opening Metathesis  
10 Polymerization of 8-Membered Cyclic Olefins. *Polym. Chem.* **5**, 3507-3532 (2014).
35. Walker, R., Conrad, R. M. & Grubbs, R. H. The Living ROMP of trans-Cyclooctene. *Macromolecules* **42**, 599–605 (2009).
36. Garber, S. B., Kingsbury, J. S., Gray, B. L. & Hoveyda, A. H. Efficient and Recyclable  
15 Monomeric and Dendritic Ru-Based Metathesis Catalysts. *J. Am. Chem. Soc.* **122**, 8168–8179 (2000).
37. Michrowska, A., et al. Nitro-Substituted Hoveyda–Grubbs Ruthenium Carbenes: Enhancement of Catalyst Activity through Electronic Activation. *J. Am. Chem. Soc.* **126**, 9318–9325 (2004).

38. Tuba, R. & Grubbs, R. H., Ruthenium catalyzed equilibrium ring-opening metathesis polymerization of cyclopentene. *Polym. Chem.* **4**, 3959-3962 (2013).
39. Kennedy, M. A., Peacock, A. J. & Mandelkern, L. Tensile Properties of Crystalline Polymers: Linear Polyethylene. *Macromolecules* **27**, 5297–5310 (1994).
- 5 40. Hester, H. G., Abel, B. A. & Coates, G. W. Ultra-High-Molecular-Weight Poly(Dioxolane): Enhancing the Mechanical Performance of a Chemically Recyclable Polymer. *J. Am. Chem. Soc.* **145**, 8800–8804 (2023).
41. Zhang, J., Matta, M. E., Martinez, H. & Hillmyer, M. A. Precision Vinyl Acetate/Ethylene (VAE) Copolymers by ROMP of Acetoxy-Substituted Cyclic Alkenes. *Macromolecules* **46**,  
10 2535–2543 (2013).
42. Ittel, S. D., Johnson, L. K. & Brookhart, M. Late-Metal Catalysts for Ethylene Homo- and Copolymerization. *Chem. Rev.* **100**, 1169–1204 (2000).
43. Ito, S., Munakata, K., Nakamura, A. & Nozaki, K. Copolymerization of Vinyl Acetate with Ethylene by Palladium/Alkylphosphine–Sulfonate Catalysts. *J. Am. Chem. Soc.* **131**, 14606–  
15 14607 (2009).
44. Carrow, B. P. & Nozaki, K. Synthesis of Functional Polyolefins Using Cationic Bisphosphine Monoxide–Palladium Complexes. *J. Am. Chem. Soc.* **134**, 8802–8805 (2012).

45. Carrow, B. P. & Nozaki, K., Transition-Metal-Catalyzed Functional Polyolefin Synthesis: Effecting Control through Chelating Ancillary Ligand Design and Mechanistic Insights. *Macromolecules*, **47**, 2541–2555 (2014).

Figures:

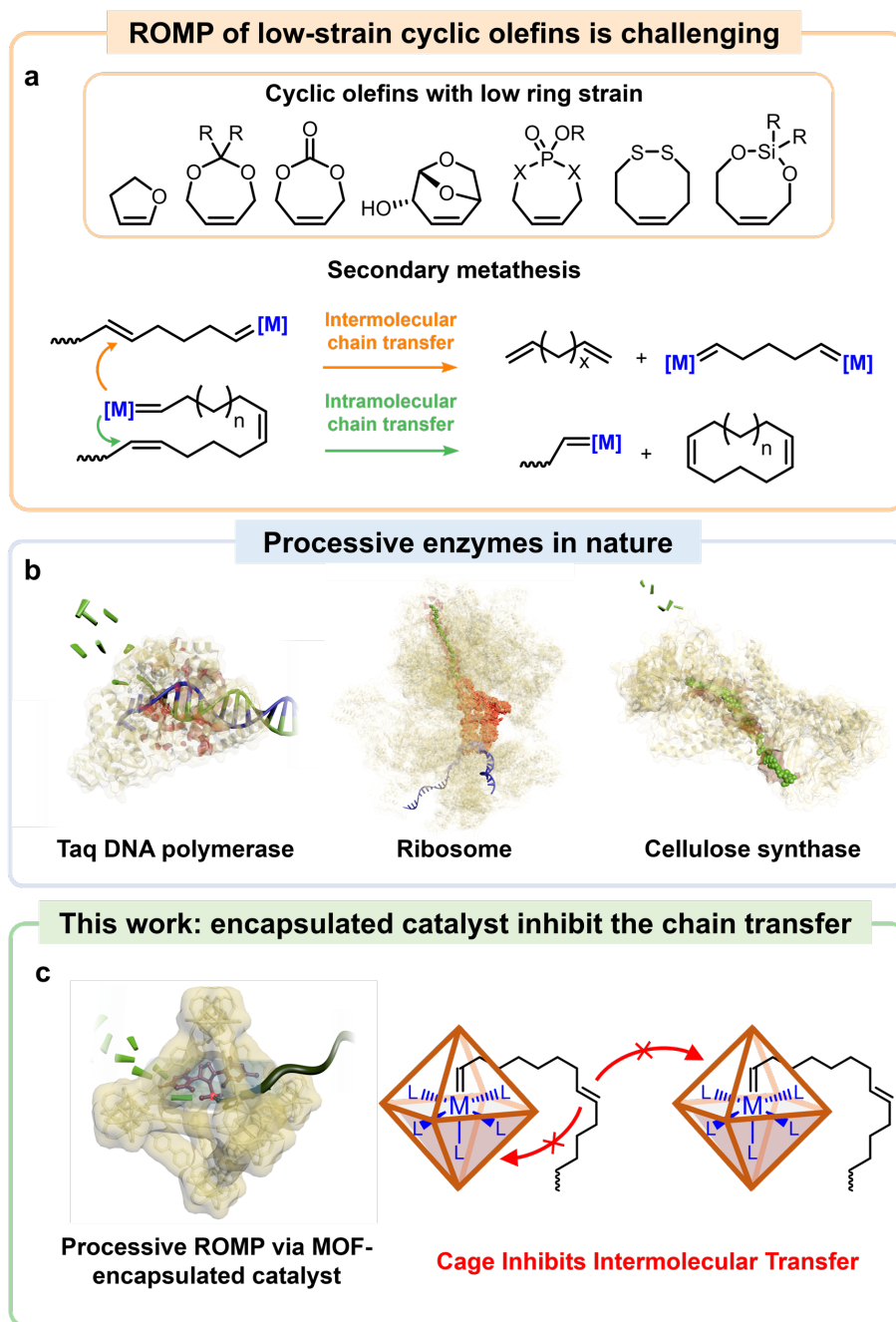


**Fig. 1. Processive ROMP via MOF-encapsulated catalyst: a bioinspired approach. (a)** Cyclic olefins with low ring strain often suffer from inter- or intra-molecular secondary metathesis. **(b)**

5 Processive enzymes and macromolecular machines that can produce ultra-high molecular weight

biopolymers are ubiquitous in nature: DNA polymerase from *Thermus aquaticus* (left) (PDB: 1QTM), human mitochondrial ribosome (middle) (PDB: 6ZM5), and cellulose synthase from *Rhodobacter sphaeroides* (right) (PDB: 4HG6). (c) The MOF cage serves as a physical barrier to protect the encapsulated catalyst from the nascent polymer, inhibit secondary metathesis, and promote processive ROMP.

5

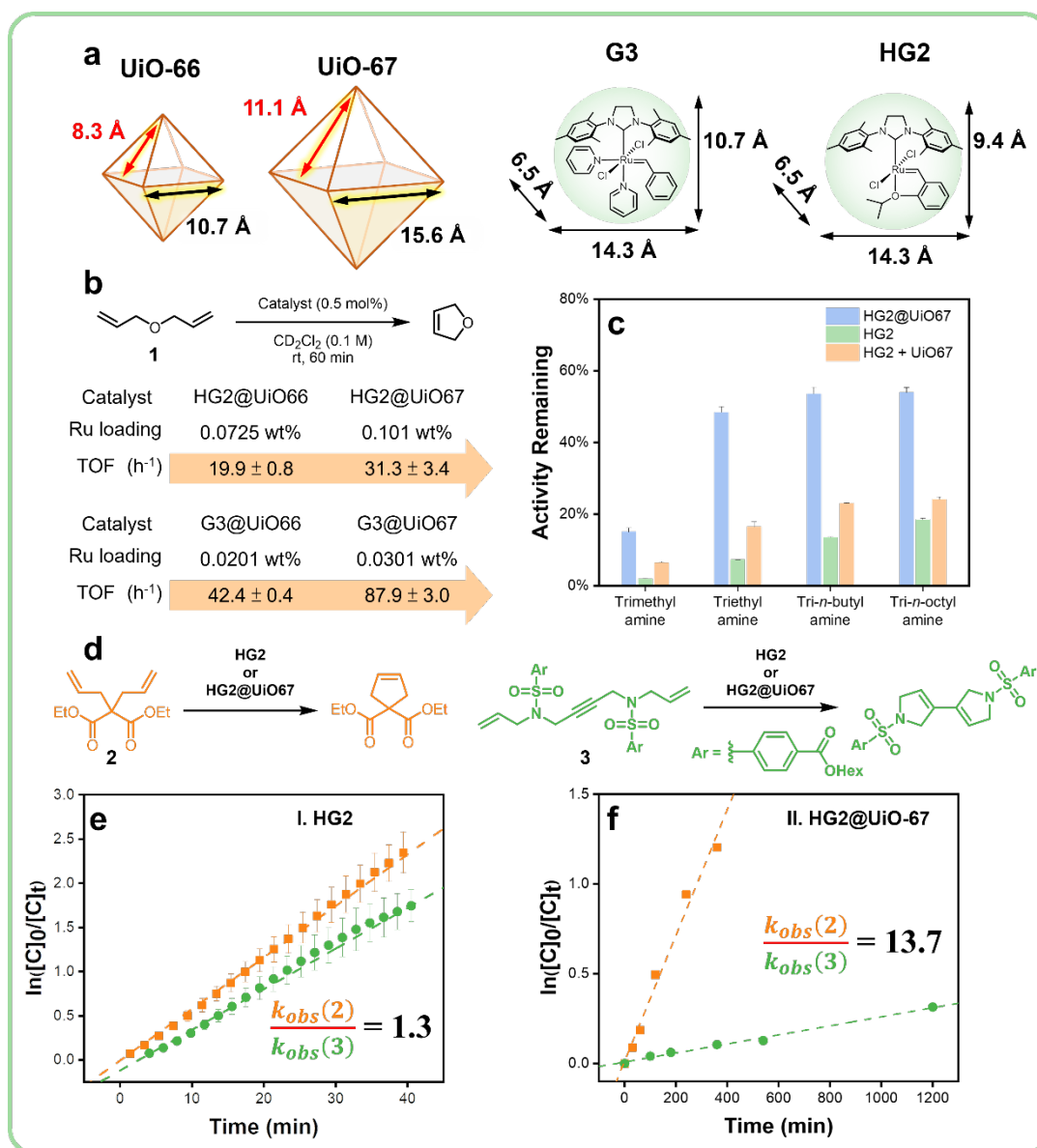


**Fig. 2. Catalyst encapsulation and activity validation.** (a) Cavity size of UiO-66 and UiO-67 compared to the size of HG2 and G3. (b) A model RCM reaction is used to evaluate the reactivities of MOF-encapsulated catalysts. (c) Remaining activities in the presence of tertiary amines of different sizes. (d)-(f) Kinetics of the RCM reactions of a small diene substrate **2** and a large enyne substrate **3** catalyzed by free HG2 (e) and HG2@UiO-67 (f).

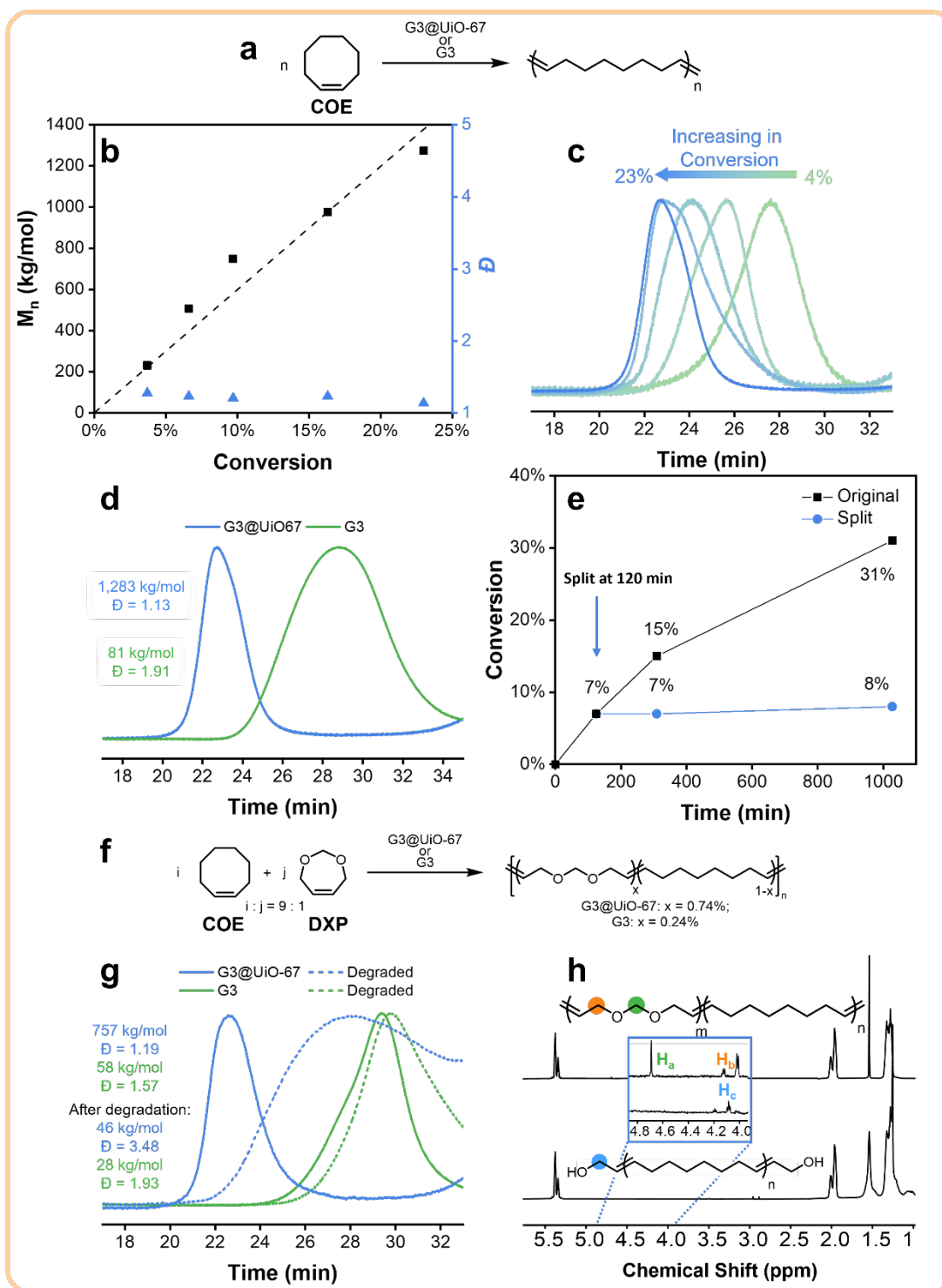


**Fig. 3. Processive polymerization and copolymerization.** (a) Equation for ROMP the cis-cyclooctene (COE). (b) The relationship of  $M_n$  and  $\bar{D}$  with respect to monomer conversion in the

ROMP of COE catalyzed by G3@UiO-67. (c) SEC traces of the polyoctenamers generated during the reaction shown in (b). (d) SEC traces of the polyoctenamers generated by G3@UiO-67 and G3 at the similar monomer conversion. (e) A ROMP reaction of *cis*-cyclooctene mediated by G3@UiO-67 was split into two equal halves at 120 min. Monomer conversion over time in the supernatant only in one half (blue) is compared to the other half in which the original mixture was kept (black). (f) Equation for copolymerization of the COE and DXP. (g) SEC traces of the copolymer of COE and DXP generated using G3 @UiO-67 and G3, and their degradation products. (h) <sup>1</sup>H NMR spectra of the copolymer of *cis*-cyclooctene and DXP generated using G3@UiO-67 and its degradation product.

10

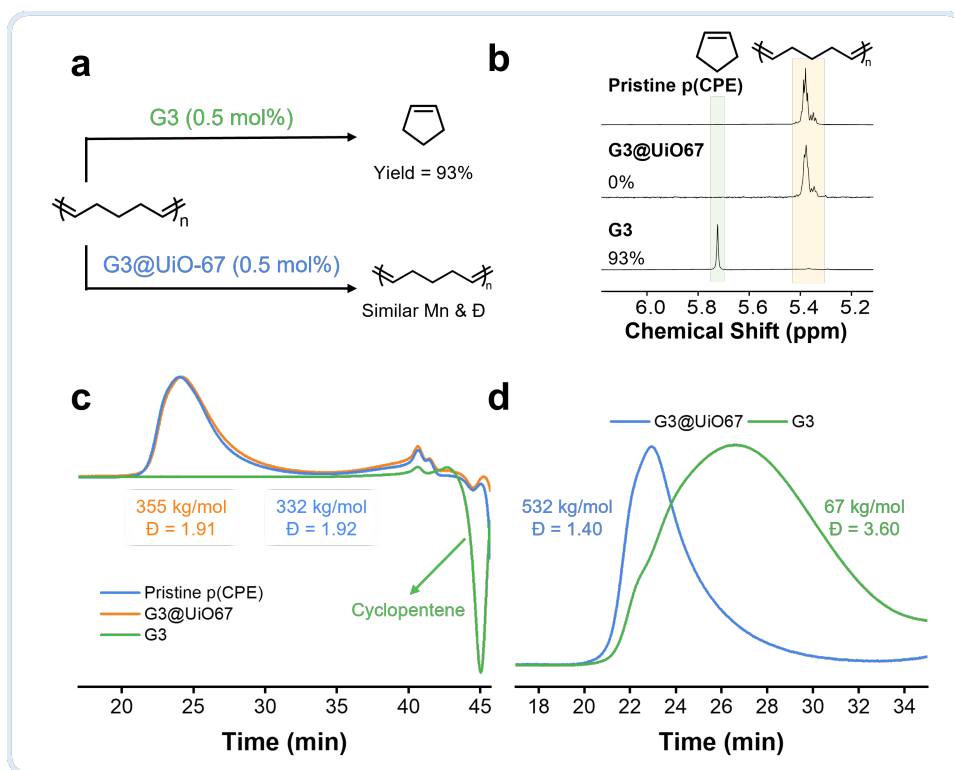


**Fig. 4. Polymerization and depolymerization of cyclopentene.** (a)-(c) The scheme (a),  $^1\text{H}$  NMR spectra (b), and the SEC traces (c) of the depolymerization of a pristine poly(pentene) mediated by G3 and G3@UiO-67. (d) ROMP of cyclopentene catalyzed by G3@UiO-67 and G3.

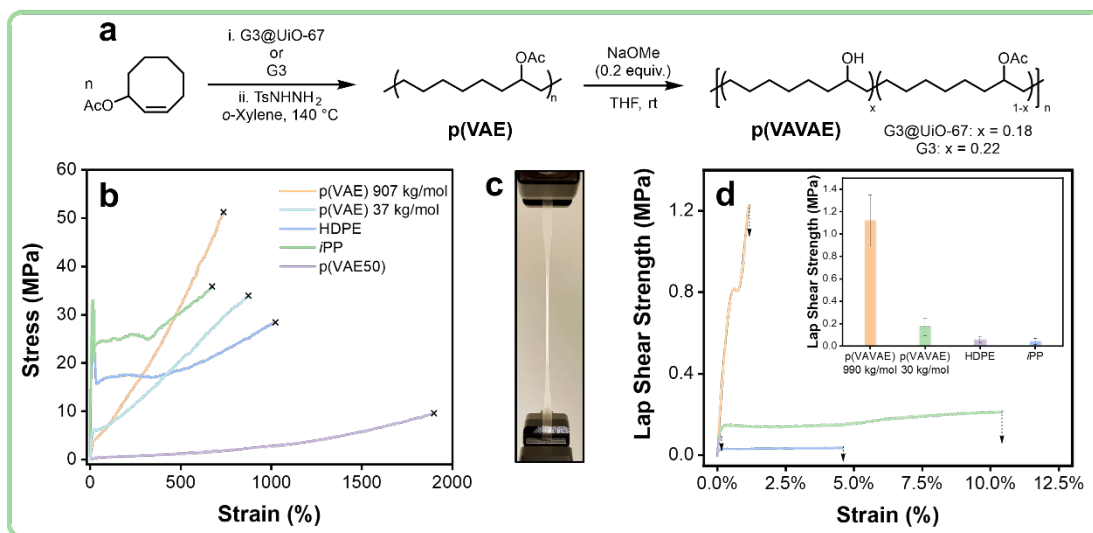


**Fig. 5. Mechanical property of ultra-high molecular weight polymers generated by G3@UiO-**

**67. (a)** Equation for synthesis of p(VAE) and p(VAVAE). **(b)** Ultra-high molecular weight

p(VAE) generated using G3@UiO-67 and p(VAE) generated using free G3 are compared to high-

5 density polyethylene (HDPE), isotactic polypropylene (*i*PP) and random p(VAE) with 50 wt%

VAc incorporation (p(VAE50)). **(c)** Image of p(VAE) (907 kg/mol) sample during tensile testing

at the onset of strain-induced crystallization. **(d)** Ultra-high molecular weight p(VAVAE) shows

6.5-fold higher lap shear strengths than the low-molecular weight p(VAVAE), and over 10-fold

higher lap shear strengths than HDPE or *i*PP. The inset shows the lap shear strengths of each

10 polymer.

## Methods:

### Synthesis of UiO-66

To a 20 mL scintillation vial, a solution of 26.6 mg of terephthalic acid in 5.0 mL DMF and a solution of 18.6 mg ZrCl<sub>4</sub> and 2.0 mL acetic acid in 3.0 mL DMF were added. The vial was sealed and heated at 100 °C in a preheated oil bath for 24 hours. After the reaction mixture was cooled to room temperature, the supernatant was removed with a glass pipette, and the white crystals at the bottom were agitated by swirling the vial gently, followed by transferring it to a conical tube. The mixture was centrifuged at 3000 rpm for 10 min. The supernatant was decanted and the fresh DMF was replenished, and the white crystals were dispersed by vortex and sonicating. The mixture was sat for 3 hours before the next round of centrifugation. Three cycles were done with DMF, followed by three cycles of washing with methanol. The crystals were transferred to a vial with a septum top and were dried at 110 °C under vacuum for 12 hours, followed by refilling with N<sub>2</sub> and cooling down to room temperature. The UiO-66 was stored under N<sub>2</sub> in a glovebox at room temperature.

### Synthesis of UiO-67

To a 20 mL scintillation vial, a solution of 19.38 mg of 4, 4'-biphenyldicarboxylic acid and 0.12 mL of triethylamine in 6.38 mL DMF and a solution of 18.64 mg ZrCl<sub>4</sub> and 1.24 mL acetic acid in 3.76 mL DMF were added. The vial was sealed and heated at 85 °C in a preheated oil bath for 24 hours. After the reaction mixture was cooled to room temperature, the supernatant was removed with a glass pipette, and the white crystals at the bottom were agitated by swirling the

vial gently, followed by transferring to a conical tube. The mixture was centrifuged at 3000 rpm for 10 min. The supernatant was decanted and the fresh DMF was replenished, and the white crystals were dispersed by vortex and sonicating. The mixture was sat for 3 hours before the next round of centrifugation. Three cycles were done with DMF, followed by three cycles of washing with methanol. The crystals were transferred to a vial with a septum top and were dried at 110 °C under vacuum for 12 hours, followed by refilling with N<sub>2</sub> and cooling down to room temperature. The UiO-67 was stored under N<sub>2</sub> in a glovebox at room temperature.

### Encapsulation of catalysts

10 HG2@UiO-66 or HG2@UiO-67: To a 20 mL scintillation vial charged with 100 mg UiO-66 or UiO-67 and a PTFE stirring bar, a solution of 10 mg HG2 in 3 mL anhydrous acetonitrile was added in a N<sub>2</sub> glovebox. The vial was sealed a screw top and tape, and the mixture was stirred for 72 hours under ambient conditions. The vial was transferred into a N<sub>2</sub> glovebox, and the mixture was poured into a conical tube, followed by the addition of 15 mL of anhydrous DCM. The mixture was vortexed and centrifuged at 3000 rpm for 10 min. The supernatant was decanted and the solid was further washed with anhydrous DCM for another 5 times. The solid was transferred to a vial with a septum cap and dried at room temperature under vacuum (0.1 mbar) for 12 hours, followed by refilling with N<sub>2</sub>. The encapsulated catalysts were stored under N<sub>2</sub> in a glovebox in the freezer. G3@UiO-66 or G3@UiO-67: To a 20 mL scintillation vial charged with 100 mg UiO-66 or UiO-67 and a PTFE stirring bar, a solution of 10 mg G3 and 6 μL 3-bromopyridine in 3 mL anhydrous acetonitrile was added in a N<sub>2</sub> glovebox. The vial was sealed a screw top and

tape, and the mixture was stirred for 24 hours under ambient conditions. The vial was transferred into a N<sub>2</sub> glovebox, and the mixture was poured into a conical tube, followed by the addition of 15 mL 200 ppm of 3-bromopyridine in anhydrous DCM. The mixture was vortexed and centrifuged at 3000 rpm for 10 min. The supernatant was decanted and the solid was further washed with 3-bromopyridine/DCM solution for another 4 times. The solid was transferred to a vial with a septum cap and dried at room temperature under vacuum (0.1 mbar) for 12 hours, followed by refilling with N<sub>2</sub>. The encapsulated catalysts were stored under N<sub>2</sub> in a glovebox in the freezer.

#### 10 **Preparation of control sample, HG2/UiO-67**

To a 20 mL scintillation vial charged with 100 mg UiO-67 and a PTFE stirring bar, a solution of 10 mg HG2 in 3 mL anhydrous dichloromethane was added in a N<sub>2</sub> glovebox. The vial was sealed a screw top and tape, and the mixture was stirred for 10 min. The mixture was poured into a conical tube, followed by the addition of 15 mL of anhydrous DCM. The mixture was vortexed and centrifuged at 3000 rpm for 10 min. The supernatant was decanted and the solid was further washed with anhydrous DCM for another 3 times. The solid was transferred to a vial with a septum cap and dried at room temperature under vacuum (0.1 mbar) for 12 hours, followed by refilling with N<sub>2</sub>. The encapsulated catalysts were stored under N<sub>2</sub> in a glovebox in the freezer.

#### 20 **Ru loading determination by ICP-OES**

Standards preparation: Six standards were prepared by dilution from commercially available zirconium ( $999 \pm 5$  ppm) standards using serial dilution in grade A volumetric glassware to cover the expected concentration ranges (50 – 2000 ppb). Digestion of encapsulated catalysts: Encapsulated catalyst (~2 mg) was weighed into a 20 mL glass scintillation vial. Concentrated hydrochloric acid (0.5 mL) was added into the vial and the mixture was sonicated until all the powder was dispersed (ca. 3 min). 2 mL of ultrapure water (Milli-Q) was added, and the mixture was sonicated for 30 min. The digested sample was diluted to 10 mL with additional ultrapure water using a volumetric flask, filtered with 0.22  $\mu$ m PTFE syringe filter, and analyzed by ICP-OES against standards.

10

### Model reactions of 1, 2 and 3

The model reaction of **1** catalyzed by different encapsulated catalysts: In a  $N_2$  glovebox, the encapsulated catalyst of designated amount (mass of catalyst was calculated based on Ru loading, 0.5 mol%) was weighted out in a 2 mL glass vial with a PTFE stirring bar. 500  $\mu$ L of dichloromethane was added into the vial and the encapsulated catalyst was thoroughly dispersed by vortex and sonication. The solid was precipitated down by centrifugation at 3000 rpm for 3 min and the supernatant was removed. In the experiments with HG2@UiO-66 or HG2@UiO-67, a solution of allyl ether (10  $\mu$ mol, 1 equiv.) in  $CD_2Cl_2$  (0.1 mL) was added to the vial, followed by dispersing the encapsulated catalyst with vortex and sonication. In the experiments with G3@UiO-66 or G3@UiO-67, a solution of allyl ether (10  $\mu$ mol, 1 equiv.) and 3,5-dichloropyridine (0.1  $\mu$ mol, 0.01 equiv.) in  $CD_2Cl_2$  (0.1 mL) was added instead. For the model

20

reactions in presence of amines, 0.5 mol% of different amines were added prior to the addition of allyl ether solution. The reaction mixture was stirred at room temperature for 1 hour and quenched with one drop of ethyl vinyl ether. The solid was precipitated down and the supernatant was taken out for analysis by  $^1\text{H}$  NMR. Turnover frequency (TOF) was calculated with the equation below.

$$TOF = \frac{\text{conversion of } 1 \times \frac{\text{amount of } 1}{\text{amount of catalyst}}}{\text{time of reaction}}$$

The model reaction of **2** or **3** catalyzed by HG2: To a solution of **2** or **3** (24  $\mu\text{mol}$ , 1 equiv.) in  $\text{CD}_2\text{Cl}_2$  (0.4 mL) in a NMR tube, a solution of HG2 (0.24  $\mu\text{mol}$ , 1.0 mol%) in  $\text{CD}_2\text{Cl}_2$  (0.1 mL) was added under  $\text{N}_2$  atmosphere. The tube was vortexed, and the reaction was analyzed with an array sampling every 2 min. Averaged conversions and standard deviations were calculated based on 3 replicates of experiments. The model reaction of **2** or **3** catalyzed by HG2@UiO-67: In a  $\text{N}_2$  glovebox, HG2@UiO-67 of designated amount (mass of catalyst was calculated based on Ru loading, 0.25 mol%) was weighted out in a 2 mL glass vial with a PTFE stirring bar. 500  $\mu\text{L}$  of solvent of reaction was added into the vial and the encapsulated catalyst was thoroughly dispersed by vortex and sonication. The solid was precipitated down by centrifugation at 3000 rpm for 3 min and the supernatant was removed. A solution of **2** or **3** (17.6  $\mu\text{mol}$ , 1 equiv.) in  $\text{CD}_2\text{Cl}_2$  (100  $\mu\text{L}$ ) was added to the vial, followed by dispersing the encapsulated catalyst with vortex and sonication. The reaction mixture was stirred at room temperature and quenched with one drop of ethyl vinyl ether at different time points. The solid was precipitated down and the supernatant was taken out for analysis by  $^1\text{H}$  NMR. The conversion was calculated based on the

integrals of protons of reactant and product, with comprehensive details provided in the Supplementary Information.

### General procedure for the polymerization by encapsulated catalysts

5 Comprehensive procedures were provided in the Supplementary Information. Procedure for the polymerization of *cis*-cyclooctene by G3@UiO-67 was stated here as an example. In a N<sub>2</sub> glovebox, 25 mg of G3@UiO-67 (mass of catalyst was calculated based on Ru loading, 1 equiv.) was weighed out in a 2 mL glass vial with a PTFE stirring bar. 500 μL of solvent of reaction was added into the vial and the encapsulated catalyst was thoroughly dispersed by vortex and  
10 sonication. The solid was precipitated down by centrifugation at 3000 rpm for 3 min and the supernatant was removed. A solution of 3-bromopyridine (1.73 μmol, 20 equiv.) in CDCl<sub>3</sub> (50 μL) was added to the vial, followed by dispersing the encapsulated catalyst with vortex and sonication. *cis*-Cyclooctene (15 μL, 115 μmol, 1330 equiv.) was added to the reaction at -10 °C. The reaction mixture was stirred at -10 °C and quenched with one drop of ethyl vinyl ether at  
15 different time points. The reaction mixture was diluted with CDCl<sub>3</sub> (0.5 mL) and the solid was precipitated down (10000 rpm, 5 min). A small portion (20 μL) of supernatant was taken out for analysis by <sup>1</sup>H NMR. The rest of the supernatant was concentrated under vacuum to ~ 0.1 mL and precipitated into 2 mL of MeOH. The precipitation redissolved and precipitated again and the polymer was analyzed by GPC and <sup>1</sup>H NMR.

20

### Synthesis of poly(vinyl acetate-co-ethylene)

Ultra-high molecular weight polymer (907 kg/mol and 990 kg/mol): In a N<sub>2</sub> glovebox, G3@UiO-67 (1.05 g, 1 equiv.) was weighed out in a 20 mL glass vial with a PTFE stirring bar. 3 mL of toluene was added into the vial and the encapsulated catalyst was thoroughly dispersed by vortex and sonication. The solid was precipitated down by centrifugation at 3000 rpm for 10 min and the supernatant was removed. Toluene (7.5 mL) was added followed by dispersing the encapsulated catalyst with vortex and sonication. 3-acetoxy cyclooctene (3 g, 17.8 mmol, 1333 equiv.) was added at room temperature and the reaction mixture was stirred for 3 hours and quenched by 0.1 mL of ethyl vinyl ether. A small portion (20 μL) of supernatant was taken out for analysis by <sup>1</sup>H NMR (conversion = 30%). The reaction mixture was diluted with 400 mL DCM, centrifuged at 12000 rpm for 10 min, filtered with 0.45 μm syringe filter, and precipitated into methanol (500\*3 mL). The precipitated polymer was dried under vacuum for 12 hours, affording a white solid (yield = 0.66 g, 21%). The condition of hydrogenation of the poly(3-acetoxy cyclooctene) was adopted from literature<sup>3</sup>, affording white to transparent solid (yield = 0.62 g, 95%). Low molecular weight polymer (37 kg/mol and 30 kg/mol): The procedure was the same as the previous literature<sup>1</sup>, except that a different amount of cis-4-octene (13.3 mg, 118.1 μmol, 10 equiv.) was used. After hydrogenation, white to transparent solid was obtained (yield = 1.35 g, 85%).

### **Synthesis of poly(vinyl alcohol-co-vinyl acetate-co-ethylene)**

Poly(vinyl alcohol-co-vinyl acetate-co-ethylene) was obtained from the corresponding p(VAE) of different molecular weights. To a solution of p(VAE) in THF (50 mM), 25wt % sodium

methoxide methanol solution (0.2 equiv. to the content of acetyl group) was added. The reaction was stirring at room temperature for 1 hour and neutralized with 0.5 HCl in methanol. The mixture was poured into a methanol solution and the white precipitate was obtained after centrifugation. The resulting polymer was dried, and a small portion was dissolved in deuterated trifluoroacetic acid overnight and integrals of the proton at the  $\alpha$ -position of the acetoxy (5.0 ppm) or the hydroxyl (5.2 ppm) were used to determine the OH content.

### Methods references

1. J. Zhang, M. E. Matta, H. Martinez, M. A. Hillmyer, Precision Vinyl Acetate/Ethylene (VAE) Copolymers by ROMP of Acetoxy-Substituted Cyclic Alkenes. *Macromolecules* **46**, 2535-2543 (2013).

### Data availability

All data are available in the manuscript or the Supplementary Information. Experimental data and characterization data for all new compounds prepared during these studies are provided in the Supplementary Information of this paper.

### Acknowledgments:

We thank Jiangwei Liu, Jing Jin, Thusitha Jayasundera, Marek Domin, Luke Perreault, Glenn R. Gaudette for characterization assistance and helpful discussions. We acknowledge the financial support provided by a grant from the National Science Foundation (CHE-2305566 and CHE-2304898) to J.N. and W.H. The research reported in this publication was supported by the National

Science Foundation Major Research Instrumentation (NSF-MRI) Program, under the award number CHE-2117246, and the HEI-S10 Program of the National Institutes of Health, under the award number 1S10OD026910-01A1.

**Author contributions:**

5 J.N., Z.Z., W.H. and C.T. designed the experiments. Z.Z., W.L., G.J.G., K.L., W.W., C.F., and A.B. performed experiments. All authors discussed the results and commented on the manuscript.

**Competing interests:**

A provisional patent based on this work has been filed by Boston College. J.N., Z.Z., W.H. are listed as co-inventors. All other authors claim no competing interests.

10 **Additional information**

Correspondence and requests for materials should be addressed to Jia Niu and Wenyu Huang.